

# Haptic Sensation-Based Scanning Probe Microscopy: Exploring Perceived Forces for Optimal Intuition-Driven Control

M. Freeman,<sup>1</sup> R. Applestone,<sup>1</sup> W. Behn,<sup>1</sup> and V. Brar<sup>1</sup>  
*University of Wisconsin - Madison*

(Dated: July 22, 2022)

We demonstrate a cryogenic scanned probe microscope (SPM) that has been modified to be controlled with a haptic device, such that the operator can ‘feel’ the surface of a sample under investigation. This system allows for direct tactile sensation of the atoms in and on top of a crystal, and we simulate, by using different SPM modalities, a sensation that is representative of the relevant atomic forces controlling the SPM. In particular, we operate the microscope in modes of (1) conventional STM feedback, (2) energy-dependent electron density imaging, (3) q-plus AFM frequency and amplitude based force sensing, and (4) atomic manipulation/sliding. We also use software to modify the haptic feedback sensation to mimic different interatomic forces, including covalent bonding, Coulomb repulsion, Van der Waals repulsion and a full Leonard-Jones potential. This manner of SPM control creates new opportunities for human-based intuition scanning, and it also acts as a novel educational tool to aid in understanding materials at an atomic level.

## I. INTRODUCTION

Scanning probe microscopy (SPM), including scanning tunneling microscopy (STM) and atomic force microscopy (AFM), is a powerful imaging technique that can be used to visualize the atomic structure of materials and the wavefunctions of electrons, as well as to manipulate individual atoms and molecules on the surfaces of materials. These imaging methods work by using piezoelectric motors with sub-Å resolution to manipulate the position of an atomically sharp tip across a smooth material surface, where tip-surface contact is maintained using a feedback loop based on tunneling current, oscillation frequency shifting, or other measurable parameters that change with tip-sample separation. Under standard operating conditions, the tip is raster scanned slowly across a surface and a full image is developed over the course of minutes to hours, depending on the specific imaging modality. More rapid, but less visual, measurements can be performed by continually scanning across the same path on the sample as some parameter is varied, or the tip can be simply parked over a specific spot of surface to monitor changes as they happen in real time. During manipulation procedures, however, the tip is carefully lowered into the surface to either change its surface structure, or to pick up atoms/molecules or trap them beneath it. Subsequent movement of atoms/molecules is performed by dragging them along the surface while moving the tip along a fixed path, or by dropping them off the tip at some desirable spot.

In all of the above operational modes, live information about the tip height and feedback parameters can be monitored by the operator by inputting their values into an oscilloscope. This allows for instantaneous changes in the tip or sample to be observed, and it also permits for precise placement of the tip relative to some surface feature by ‘blindly’ moving

the tip in sub-Å steps and monitoring — for example — the tip height as it is altered by individual surface atoms. This later capability allows for manipulation to be performed without first obtaining sub-Å resolved images, which would be prohibitively time consuming. During manipulation itself, a live feed of the scanning parameters is necessary for assessing if an atom/molecule is on the tip — which appears as a change in height — or if an atom/molecule is following the tip — which can be known by observing the current noise; while an oscilloscope can be used for such observations, it is more common to convert the tunneling parameters into an audible sound with, for example, the tip height and tunneling current represented by a particular pitch. This approach is often more intuitive and, in some cases, can provide a clearer picture of the tip and sample conditions.

Recently, commercial haptic feedback technologies have proliferated as a effective way in which to interact with a virtual space. Haptic feedback arms allow a user to move a cursor in a simulated 3D space, where contact with a virtual object results in a force imparted on the hand of the operator. These devices are used extensively as tools for designing 3D graphics/sculptures, performing robot-assisted surgeries, training for medical and dental operations, controlling robot arms in dangerous environments, and other applications.<sup>1</sup> They can be interfaced with any tool that exhibits motor-controlled  $xyz$  motion and provides some positional feedback.

Shortly after the innovation of piezo-controlled SPMs, efforts were made by several groups to interface them with haptic control arms as a way to ‘feel’ the surfaces being probed.<sup>2–6</sup> Those experiments, which included both STMs and AFMs, allowed users to feel coarse features on the surfaces of materials, including protruding quantum dots and step edges, with characteristic heights as small as 2nm. Subsequent demonstrations showed that haptic-controlled AFMs could be used to sense and manip-

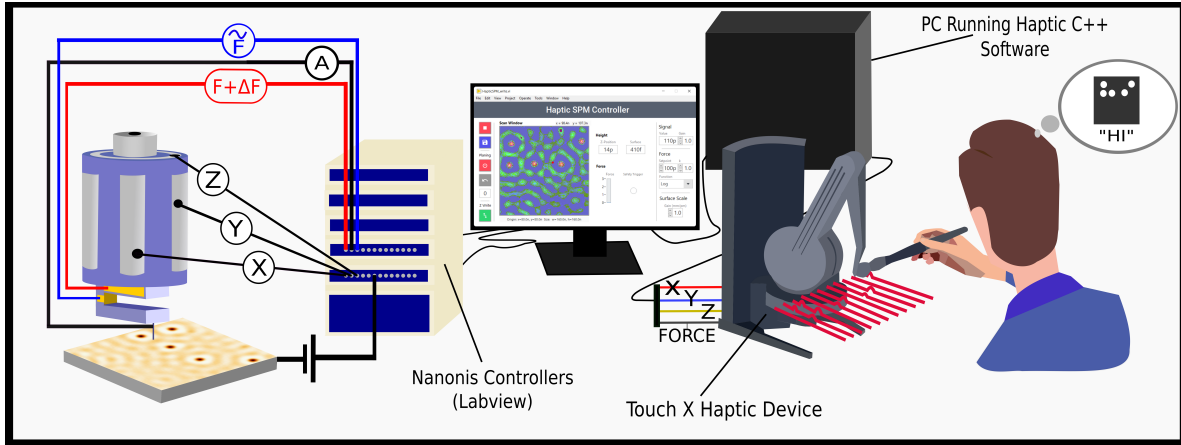


Figure 1. The operational setup used for the haptic-SPM controller. The haptic device, controlled via a dynamic-link library written in C/C++, and the Nanonis control hardware, controlled via Nanonis’s SPM control software, both connect to a desktop computer. Both of these interface via a LabVIEW program on the computer, which handles signal processing and the main GUI. The user moves the pen, and the xy-positional data from the haptic device is mapped to control the xy-position of the pen (in some modes, the z-positional data is also mapped). Meanwhile, signals like the tip z-position, tunneling current, or cantilever frequency shift are converted into a force, applied to the haptic device, and felt by the user.

ulate carbon nanotubes and large biomolecules, such as viruses, fibrin, and DNA.<sup>5,7–12</sup> These experiments allowed the sensing of both lateral and vertical tip-sample forces as small as 1nN.<sup>9</sup> Later implementations also showed how haptic-controlled AFMs could be used to precisely position micron-sized beads,<sup>13–16</sup> sense semiconductor devices,<sup>13</sup> and sense the distance dependence of AFM tip-surface interactions. These later experiments were particularly useful for instructional purposes; the analogous nature between tip-surface and pen-hand interactions made it easier for students to understand forces between material interfaces.<sup>17–20</sup>

Most early haptic-SPM experiments were performed in ambient conditions, where it is difficult to maintain consistent tip and sample conditions, and where surface adhesion forces introduced from interfacial molecules can be significant. Haptic experiments using optical tweezers provided a means of bypassing those challenges, with demonstrations showing reliable manipulation of trapped beads near around barriers, and force sensing down to 1pN.<sup>21–23</sup> More recently, ultra-high vacuum (UHV) STM measurements — where surface impurities were eliminated — that included haptic arm control were performed on atomically smooth Au(111) surfaces with adsorbed C<sub>60</sub> molecules.<sup>24</sup> That work demonstrated that when STM feedback is controlled with tunneling current rather than tip-sample forces, the tunneling current could reliably be used to control the haptic arm force, allowing the operator to feel atomic step edges, and to even manipulate C<sub>60</sub> molecules. Though lacking force-feedback, experiments using infrared cameras mapped three-dimensional hand movement to AFM tip movement, and were able to manipulate a PTCDA monolayer on an atomically

smooth Ag(111) surface.<sup>25,26</sup>

Here we expand on those previous works by integrating a haptic feedback arm with a cryogenic, UHV SPM equipped with a quartz tuning fork sensor that can be used for both operation as an AFM and STM. The ultra low temperature environment of the surface enables highly stable scanning conditions that we utilize to demonstrate several operational modes including the linking of the haptic force to (1) tunneling current, (2) changes in tuning fork frequency and (3) local electron density. We also explore the use of different feedback-force (‘feeling’) functions, which create different tactile sensations that can be used to mimic different atomic forces, and to optimize the ease of operation. Additionally, we also demonstrate the ability to manipulate the positions of individual CO molecules with atomic resolution, such that the operator can feel as the molecules skip between atomic lattice sites.

## II. METHODS

### A. Hardware and Software

All measurements were performed in a commercial SPM (CreaTec GmbH) with Nanonis (SPECS GmbH) electronics and software. The SPM is operated in UHV conditions at 4.5K using a qPlus quartz tuning fork sensor for dual AFM/STM imaging. A Touch X haptic device from 3D Systems was used for all experiments performed. The device is operated via device drivers, calibration software, and the OpenHaptics 3.5 application programming interface (API) for the C/C++ languages. It possesses a positional resolution of 1100 dots per inch (dpi), a workspace of

160 W × 120 H × 120 D mm, and a maximum force output of 7.9 N, nearly double the resolution of haptic devices used in previous experiments<sup>24</sup>; the high resolution is ideal for obtaining smoother-feeling surfaces and forces.

There are three interconnected software components that allow the haptic device to communicate with the STM/AFM:

(1) The Nanonis SPM control system, which is controlled through a LabVIEW-accessible API, and allows signal values (e.g. tip positional data, current, and oscillation frequency shift) and control parameters (e.g. tip position, tip bias) to be read and controlled in LabVIEW; (2) a custom dynamic-link library developed using the OpenHaptics API, and coded in C++, which allow positional and force parameters to be read and written to the haptic device via LabVIEW; and (3) a LabVIEW GUI program used to interface the two, processing signals from each device. The LabVIEW GUI, library, and all relevant data can be found at [www.github.com/HapticSPM](http://www.github.com/HapticSPM).

The synthesis of these hardware and software components results in the complete haptic controller. Here, we further discuss the varying modes of the controller, and the methods used to fine-tune their operation.

## B. Operational Basics

There are two general modes of operation with which experiments were preformed: *read mode* and *write mode*. In read mode, the haptic pen only controls the tip motion in the horizontal  $xy$  plane. The force on the haptic pen is determined by reading the signal of interest and referencing it to the  $z$ -position of the haptic pen: if the pen travels below a virtual, scaled version of the sample, it is pushed upwards. The ‘feel’ of the sample (i.e., force as a function of distance) is purely virtual, and determined by a function of the form

$$Force = f(signal, z_{pen}), \quad (1)$$

where *signal* is the signal of interest (e.g., tip  $z$  position, LDOS, cantilever frequency shift, etc.), and  $z_{pen}$  is the  $z$  position of the haptic pen in mm. By adjusting the parameters of this function, the overall ‘feeling’ of the sample can be changed, as described in Sec. IV. This mode of operation is similar to the ‘augmented reality mode’ used in previous haptic-AFM implementations.<sup>9,27</sup>

Meanwhile, in write mode, the haptic pen controls the horizontal  $xy$  motion as well as the vertical  $z$  motion of the STM/AFM tip. The force on the haptic pen

is determined by a function

$$Force = f(signal), \quad (2)$$

which is entirely dependent on the signal of interest, such as tunneling current, local density of states, or change in oscillation frequency ( $\Delta F$ ). As an example, if the tunneling current is the signal of interest, then as the pen (and thus, tip) moves downwards and approaches the surface, the tunneling current increases; this current is converted to an upwards force, which the user interprets as a hard surface.

The force functions given by equations 1 and 2 varied depending on the signal of interest, and are described explicitly in the next section.

In normal use, a square region of interest is chosen on a samples’ surface using the standard Nanonis SPM control software. This region’s location and size are then used by the haptic device to convert the millimeter-scale horizontal movement of the pen to the nanometer-scale horizontal movement of the tip. The workspace of the pen is confined using hard-coded, vertical walls to a 16 cm × 16 cm horizontal area in the middle of the pen’s range of motion. This effectively confines the user of the haptic device to the particular region of interest on the sample.

The sample surface is often slanted relative to the axes of movement of the scanning probe, and a planing algorithm is used to ‘flatten’ the surface, such that the horizontal movement of the pen is mapped to tip movement along the plane of the surface. This algorithm is implemented by having the user choose 3 points on the sample by pressing the pen into the surface until a certain force threshold is reached; these points are used to calculate a plane of best fit.

This plane of best fit is utilized differently in each mode. When the device is in read mode and controller feedback is on, the signal is simply mapped to this plane of best fit, flattening the surface for the user without controlling the tip  $z$  position. When the device is in read mode and controller feedback is off, the tip  $z$  position is controlled by the device, but constrained to movement along the plane of best fit. When the device is in write mode, the tip  $z$  position is completely controlled by the device, and is mapped in such a way that purely horizontal movement on the device corresponds to tip movement purely along the plane of best fit.

In write mode, the vertical  $z$  position of the pen is further processed. The tunneling current as a function of distance from the surface is exponential, and rises from 1 pA to 10 nA over the range of a few hundred of picometers. Since the force applied by the haptic device is a function of this parameter, it was necessary to implement a function that further scaled the  $z$  motion of the haptic device. This allows for a larger range of motion (on the order of hundreds of picometers) when far above the surface, while also allowing for a finer range of motion (on the order of picometers) when near the surface. The function used was

$$z_{stm}(z_{pen}) \sim \begin{cases} b(\exp(\frac{1}{b}[z_{pen} - z_{thresh}]) - 1) + z_{thresh} & z_{pen} \leq z_{thresh} \\ z_{pen} & z_{pen} > z_{thresh} \end{cases} \quad (3)$$

where  $b$  is a scaling constant (nm), and  $z_{thresh}$  (nm) is the  $z$ -position at which the tunneling current surpasses above the background noise level of current (chosen to be about 10 pA). This function acts as a configurable ‘floor’ for the pen, past which the STM/AFM tip can only travel a few tens of picometers, regardless of how much further the haptic pen position  $z_{pen}$  travels.

In both modes, it is possible to configure the perceived height of features on the surface by changing the desired level of positional scaling, which allows the user to feel differently-sized surface features. Thus, larger surface features like step-edges and smaller features like individual molecules/atoms are able to be felt in a more user-friendly way, without sacrificing the ability to feel one or the other.

Finally, a drag force was implemented to smoothen the user’s movements in an attempt to eliminate all but deliberate pen motions. This force was determined by the function  $\mathbf{F}_{drag} = -c\mathbf{v}$ , where  $\mathbf{v}$  is the velocity of the haptic device cursor and  $c$  is an arbitrary constant. As an additional safety measure, the maximum speed of the STM/AFM tip could be configured such that the tip is only allowed to travel at less than a given speed. Beyond limiting unwanted rapid motions of the STM/AFM and the haptic device, this feature was found to be essential for fine-grained operations like molecular manipulation.

### III. MODES OF OPERATION

We tested our haptic-SPM controller on an atomically flat Cu(111) surface cleaned by repeated cycles of sputtering with Ar ions (500 V, 7  $\mu$ A) for 10 minutes and annealing around 400 C for ten minutes. The crystal was allowed to cool after annealing cycles and before the next sputter. After loading the sample into the SPM, carbon monoxide molecules were deposited on the sample *in situ* via a UHV leak valve.

#### A. STM Topography-Based Force

In this operational mode, the STM feedback controller remains on, adjusting the  $z$ -position of the tip to maintain a constant ‘setpoint’ current. The haptic controller is operated in read mode, such that the haptic pen controls only the  $x$  and  $y$  positions of the STM tip. The force exerted on the pen is determined by the function

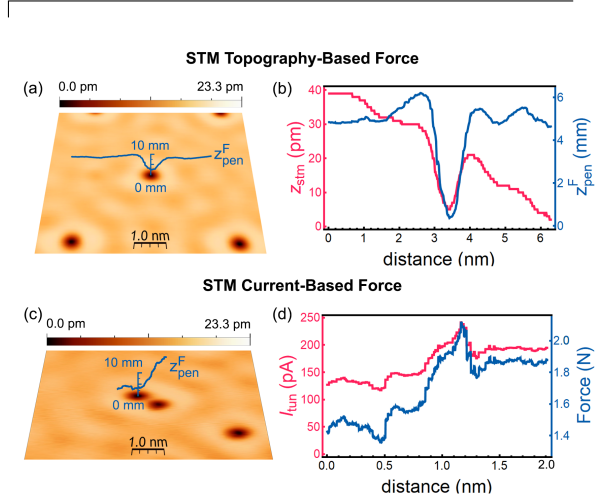


Figure 2. An example of the two STM-based modes in which the haptic pen was operated. The pen position is plotted in three dimensions alongside the corresponding STM imagery is shown in both (a) and (c); a comparison of this is shown in (b), and a comparison of force vs tunnelling current is shown in (d).

$$f(z_{pen}, z_{stm}) = \begin{cases} k|z_{pen} - az_{stm}| & z_{pen} \leq az_{stm} \\ 0 & z_{pen} > az_{stm} \end{cases}, \quad (4)$$

where  $z_{pen}$  is the vertical position of the haptic pen in mm,  $z_{stm}$  is the height of the tip relative to the plane of best fit in nm,  $a$  is the gain of the input signal in mm/nm, and  $k$  is the stiffness of the plane in N/m.  $az_{stm}$  can be understood as the STM tip height read and projected into the virtual haptic space.

The nature this function is that when the haptic pen is held ‘above’  $az_{stm}$  it experiences no force, but as the position of the pen hits  $az_{stm}$  and then goes below it, it experiences a spring force with an adjustable stiffness  $k$ . We note that many different functions could be used to generate the perceived force and in Section IV we explore the impact of how different functions affect the haptic sensation. Since the pen can move above  $az_{stm}$ , its  $z$  position may or may not correspond to the surface topography. Thus,  $z_{pen}^F$  is used to distinguish the case in which the user is applying a constant finite downward force on the pen; the pen height would then more closely correspond to the surface topology.

Fig. 2a shows the three-dimensional path of the haptic device ( $z_{pen}^F(x_{pen}, y_{pen})$ ) acquired using this mode of operation while transiting a carbon monoxide (CO) molecule on Cu(111). The data is plotted alongside the STM surface topography, and Fig. 2b directly compares a linecut of the STM topography



to  $z_{pen}^F(x_{pen}, y_{pen})$ , showing good agreement, indicating that the haptic pen is able to reliably feel sub-nanometer features.

There are a few factors that can account for discrepancies between the haptic pen position and the STM position. First, the STM topographic data contains a slope that is representative of the actual slope of the sample, while the path of the haptic pen is flat. This is due to the slope correction algorithm we implemented, described in Section II B. Second, there is a 1 - 10 ms delay between when the STM signal value changes and when the haptic device writes the corresponding force. Also, an applied force does not immediately change the position of the pen; it takes time for the user to react to this force and adjust the pen position accordingly. Thus, the faster the tip traverses, the more out-of-sync the pen will be from the STM signal. Additionally, piezo drift can cause a shift in tip position between measurements, which could account for a small amount of discrepancy between the STM imagery and the path traversed.

## B. STM Current-Based Force

The next method of operation we describe implements a current-based force, where the STM feedback is turned off and the haptic controller is operated in write mode, meaning the pen controls the tip position in all dimensions. The arm produces an upwards force proportional to the tip tunneling current, which increases with decreasing tip-sample separation. The force function used is

$$f(I_{tun}) = I_{tun}/I_{set} \quad (5)$$

where  $I_{tun}$  is the tunneling current,  $I_{set}$  is an arbitrary current chosen by the user, which the pen tends to maintain during use.

Since the tunneling current as a function of proximity to a surface is exponential, the force being felt by the user is also exponential; however, when the composition of equations 3 and 5 is considered, force as a function of pen height is at first exponential, then becomes linear as the force approaches the maximum force. We found setting the tip force directly to the tunneling current created difficult operating conditions, where small changes in tip height led to large changes in force that the haptic arm could not produce at sufficient rates to maintain stable tunneling; it was also difficult to avoid tip crashes since the maximum force of the haptic pen could easily be reached with small changes in the tip height. The effect of Eq. 3 is to prevent such problems by dramatically decreasing the degree to which the haptic arm moves the pen towards the surface after a certain threshold height is met. This correction also allows the operator to maintain a constant tip height at  $z_{thresh}$ , since the transition to different functional forms on either side of  $z_{thresh}$

can be easily felt by the user.

A representative contour of  $z_{pen}(x_{pen}, y_{pen})$  obtained using a current-based force is shown in Fig. 2c, along with the corresponding topography obtained using standard STM imaging. We find that the topography is less-well reproduced in comparison to using a topography-based force (read mode), and we attribute that difference to the 1 - 20ms communication delay between the haptic pen and STM, which makes it difficult for the user to maintain a perfectly constant current. Fig. 2c, meanwhile, compares the force on the haptic pen against the tunneling current as the user traverses the tip across an individual CO molecule. Here we find good agreement, with the current/force decreasing as the tip moves into the CO-defined dip (due to the tip moving further from the surface as it goes off an edge) and increasing as it moves out.

## C. STM LDOS-Based Force

The tip-sample distance in an STM is typically maintained by using the tunneling current as the feedback parameter, however, the force on the haptic arm can be defined by any measurable value. For example, the energy dependent local density of electronic states (LDOS) is one property that is commonly measured in STM experiments to provide direct visualization of electron wavefunctions and scattering patterns. The LDOS at any particular point of the sample is proportional to the tip-sample conductance at the tunneling voltage, and is commonly measured using a lock-in amplifier. By converting the lock-in signal to a force written to the haptic controller operating in read mode, the user is able to feel the local electron density as it varies across the sample.

Formally, this mode of operation is equivalent to replacing the variable  $z_{stm}$  in Eq. 4 with  $LDOS_{stm}(V)$ , and the gain variable  $a$  having units of mm/V (the lock-in outputs a voltage that is proportional to the sample conductance). Thus, the contour felt by the operator,  $z_{pen}^F(x_{pen}, y_{pen})$ , is defined by the local sample conductance, which depends on the tunneling bias. An example is shown in Fig. 3a, where  $z_{pen}^F(x_{pen}, y_{pen})$  of a particular path is plotted on top of an LDOS image of the Cu(111) surface, which reveals standing waves created by the interference pattern of the copper surface state. Fig. 3b, meanwhile, directly compares the trajectory of the haptic pen with the corresponding linecut of the LDOS image, showing excellent agreement.

We note that, unlike STM-derived topography, the LDOS changes dramatically with the applied bias, and those changes reveal the rich behavior of the electrons in the material. In the case of Cu(111), LDOS images taken at higher/lower sample biases reveal shorter/longer wavelength standing wave patterns due to the different momenta of the participating electrons. Moreover, LDOS images of molecules can

reveal the internal structure of the different molecular orbitals.<sup>28–31</sup> Such rich behavior is all accessible to haptic force based sensing.

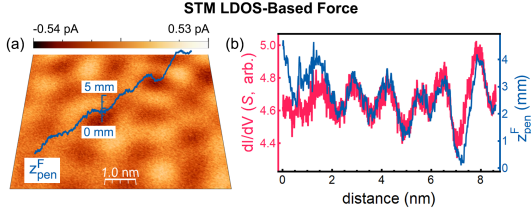


Figure 3. An example of the LDOS-based mode in which the haptic pen was operated. The pen position is plotted in three dimensions alongside corresponding LDOS imagery is shown in (a); a direct comparison is shown in (b).

#### D. AFM Topography-Based Force

In this mode of operation, the feedback of the system remains on, and the tip-sample distance is maintained at a constant height by linking the feedback to the frequency shift of the AFM cantilever ( $\Delta f$ ), which changes depending on the tip-sample distance, and the specific tip-sample interactions (i.e. electrostatic, Van der Waals, etc...). The haptic controller is operated in read mode, with  $x$  and  $y$  positions of the AFM tip controlled directly via the pen, and the force

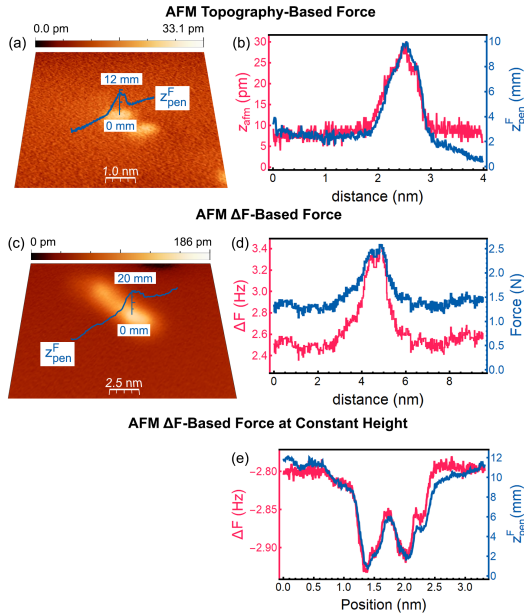


Figure 4. An example of the three AFM-based modes in which the haptic pen was operated. The pen position plotted in three dimensions alongside the corresponding AFM imagery is shown in (a) and (c); a direct comparison is shown in (b) and (e), while (d) compares frequency shift and force.

on the pen is set by Eq. 4, where  $z_{stm}$  is replaced by  $z_{afm}$ .

Figure 4(a) shows the three-dimensional path of the haptic pen with constant force ( $z_{pen}^F(x_{pen}, y_{pen})$ ) acquired using an AFM topography based force while transiting over a CO molecule on Cu(111). The data is plotted atop the associated AFM image, and Fig. 4(b) directly compares  $z_{pen}^F(x_{pen}, y_{pen})$  to a linecut of the topography.

We note that, unlike the STM topography image where the CO molecule are felt as dips (Fig. 2a,b), in AFM mode the molecules are perceived as protrusions. This is because the molecules lower the local conductivity of the sample, but they increase tip-sample interactions. Thus haptic-controlled AFM allows the user to better sense the physical topology of the sample.

#### E. AFM $\Delta F$ -Based Force

Comparable to Section III B, the pen was operated in write mode, using a force based on frequency-shift in place of a force based on tunneling current. The function used was

$$f(\Delta F) = \begin{cases} 0 & \Delta F \leq \Delta F_{setpoint} \\ k \log(\Delta F / \Delta F_{setpoint}) & \Delta F > \Delta F_{setpoint} \end{cases}, \quad (6)$$

where  $\Delta F$  is the frequency-shift,  $\Delta F_{setpoint}$  is an arbitrary frequency-shift chosen by the user, at which the pen begins to feel a force, and  $k$  is an arbitrary scalar. We note that if the force on the pen is linked directly to  $\Delta f$ , the applied force on the pen is maxed out too quickly and the operator can easily crash the tip. Using the logarithmic, step-like form shown in 6 makes it easy to hold the tip at a particular setpoint, while still enabling tip-sample force perception as the tip is lowered further.

The haptic pen transiting a molecule in this mode is shown in Fig. 4c, exemplifying that passing over a molecule correlates causes the user to feel a bump in the surface. Fig. 4d shows that there is a clear correlation between frequency-shift and the force being written to the arm. The major benefit of this mode of operation is that the pen force is directly linked to the actual physical force between the tip and sample (which establishes  $\Delta f$ ). This allows the user to actually feel different tip-sample forces, depending on the value of  $\Delta F_{setpoint}$  used, which has previously been shown to be valuable in educational settings.<sup>17–20</sup>

#### F. AFM $\Delta F$ -Based Force at Constant Height

The last mode of operation we demonstrate is frequency-shift based, for which controller feedback was turned off, but the tip is fixed to move in a flat plane that is established by fitting topographic data

obtained first by imaging the surface in standard feedback mode. Local changes in surface topology raise or lower the frequency shift from resonance of the AFM cantilever and this signal was converted to a force on the haptic device in read mode. This method of imaging has been shown to be useful in obtaining highly resolved images of atomic bonds within molecules.<sup>32</sup>

The force on the haptic pen transiting two CO molecules in this mode is shown in Fig. 4e, plotted atop the associated direct measurement of  $\Delta F$  from the Nanonis software. We note that here we plot the raw value of  $\Delta F$  rather than the absolute value, which would reveal peaks instead of dips.

#### IV. FEELING FUNCTIONS

Determining how the surface ought to feel when using the haptic controller is an important, yet highly subjective task. A common choice is to use the input signal as the basis for the force curve, and either use the signal itself or a scaled version of it to determine how the surface feels.<sup>24</sup> This method, however, may not be the most ergonomically sound solution. The only technical constraint of the 'feeling function' used is that it must prevent drastic force vs. tip height dependencies which can lead to unstable operation. But, otherwise, there is substantial leeway in choosing a function that either feels best to the user, or is chosen to mimic a particular interatomic force. In the later case, the force felt on the pen would represent the forces that a theoretical atom with a particular wavefunction and charge state would feel if scanned across the surface.

Studies report that the psychometric function for compliance discrimination (i.e., perceived stiffness as a function of the actual stiffness) is roughly logarithmic, and on the order of N/mm.<sup>33</sup> This seems to suggest that force-functions will yield significantly different perceptions than what might be initially predicted; just because force as a function of distance is exponential, for example, doesn't mean the surface will 'feel exponential' to the user.

To investigate this, several force functions that simulate various forces in nature were explored. These functions were of the form

$$f(r) = \begin{cases} \varphi(r) & r \geq 0 \\ 0 & r < 0 \end{cases}, \quad (7)$$

where  $r \equiv az_{stm} - z_{pen}$  is defined to be the penetration distance, and  $f(r)$  takes on the various forms as described below. The constants  $\rho$ ,  $\tau$ ,  $\sigma$ , and  $\epsilon$  were all chosen to provide the a force curve confined to a 30 mm range between zero force and the maximum force (3 N). The force from each function while transiting a CO molecule is plotted in Fig. 5. Since describing

these forces is necessarily both subjective and qualitative in nature, descriptions of each function are provided alongside each transit plot.

#### V. MANIPULATION

Controlled manipulation of single atoms and small molecules with an STM is often an arduous and time consuming task. Haptic controllers are especially useful for such a use-case; the user can find the target atom/molecule and perform manipulation without having to conduct a time-intensive raster scan after each manipulation attempt.

Manipulation of CO molecules on a copper surface using the haptic device was achieved. To accomplish this, a user operates the pen in height-based read mode to position the STM tip directly over the center of a CO molecule. Once the tip is centered, lateral control of the haptic arm is momentarily paused (to minimize chances of kicking the molecule to another lattice site instead of picking up the molecule in a controlled fashion). Next, the setpoint current (the particular value of current maintained by the STM feedback) is raised to roughly 9.98 nA and the bias is lowered to 700  $\mu$ V, effectively bringing the tip significantly closer to the molecule. Concurrently, a graph on the LabVIEW GUI displays the z-position of the tip; when several oscillations are observed, then it is likely that the molecule has transferred from the sample to the tip. Lateral movement is then re-enabled, and the user can 'drag' the molecule to the desired location. Once this location is reached, the bias is then raised to 50 mV, and the setpoint current is decreased, raising the tip and causing the molecule to jump back to the surface.

It has been demonstrated that picking up CO molecules can change the chemical properties of the STM tip,<sup>34</sup> meaning that surface features not typically discernible under normal operations can be felt via the haptic device. CO molecules are polar, and thus have a tendency to be attracted to interfacial sites on the copper surface; the molecule will 'skip' or 'jump' between these sites as the tip-molecule pair traverse the sample. With a high gain setting on the haptic controller, each of these jumps can be distinctly felt by the user.

Fig. 6a maps the configuration of the STM tip, CO molecule, and Cu lattice relative to what was felt by the haptic pen, shown in Fig. 6b. The lattice constant of a Cu fcc lattice is 3.597 Å,<sup>35</sup> which is consistent with what is felt by the haptic device. Images before and after manipulation are also shown in Fig. 6c, with the latter spelling out 'hi' in braille.

## Feeling Functions while Transiting a CO Molecule

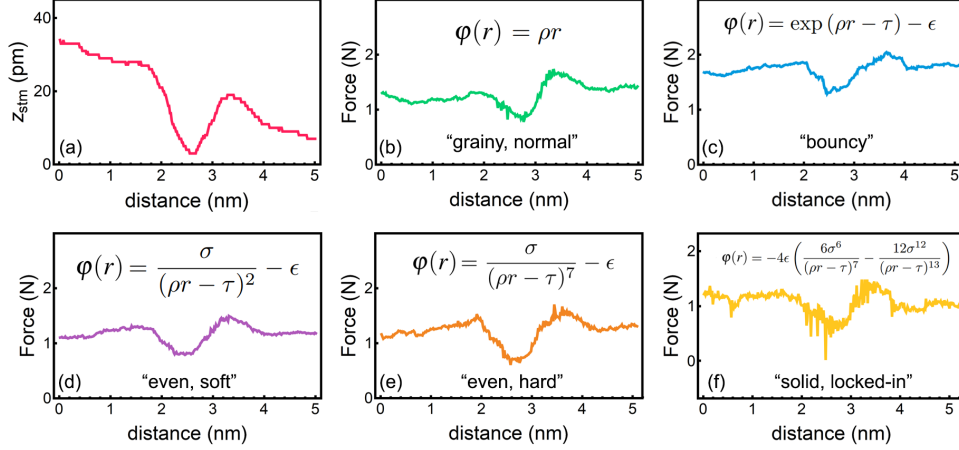


Figure 5. An example of the forces experienced while transiting a CO molecule. A linecut of the molecule is shown in (a); a comparable path was taken with the haptic pen applying a (b) linear force, (c) covalent bonding force, (d) Coulomb force, (e) Van der Waals force, and (f) Leonard-Jones force.

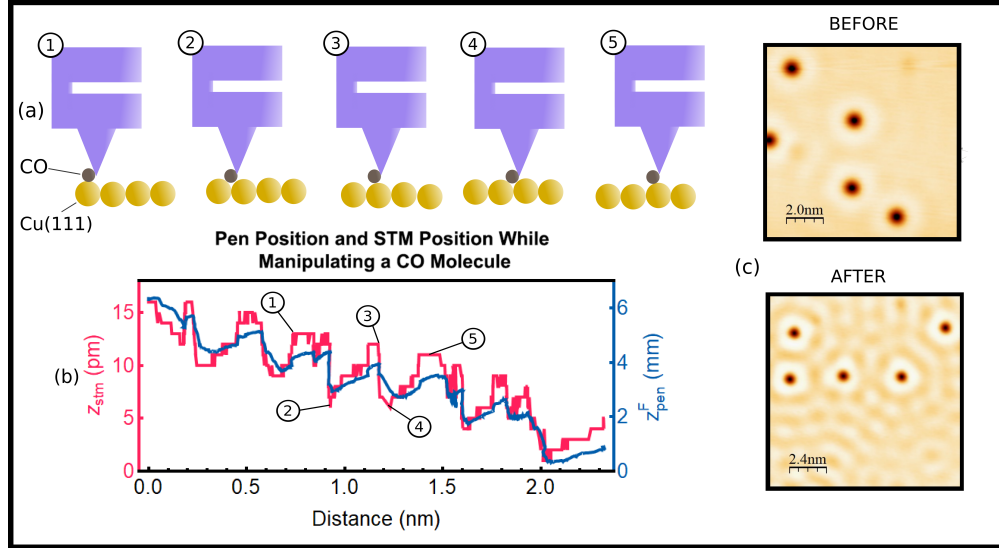


Figure 6. An example of controlled manipulation of CO on Cu(111) using the haptic device. Shown is (a) the mechanics of how controlled CO manipulation works (b) data showing that corrugations of a size consistent with the Cu(111) lattice spacing are able to be felt with the haptic device, and (c) before and after images of the same area, in which CO molecules were moved to spell out ‘hi’ in Braille.

## VI. DISCUSSION AND OUTLOOK

A significant limitation of the specific haptic device used is its relatively small range of motion in the  $xy$  plane. Operations were limited to a  $16\text{ cm} \times 16\text{ cm}$  area, meaning that, for a large enough area of interest, small surface features were scaled down significantly and were more difficult to feel. A haptic device with a larger range of motion could address this issue, perhaps by keeping the scale of horizontal movement constant, and increasing/decreasing the allowed range of motion for larger/smaller areas of interest, respec-

tively. This would effectively allow the user to feel both large and small surface features at the same time, without sacrificing movement range for surface scale.

Additionally, a haptic device with a higher operating frequency ( $>1\text{ kHz}$ ) would be much better equipped to handle fast, significant changes in force. The haptic controller presented in this paper uses relatively soft force curves in order to account for high-frequency changes in signal; faster technology could allow surfaces to feel significantly harder.

Regardless of these technological limitations, however, the haptic controller described in this paper pro-



vides a useful and intuitive way of interacting with a UHV, low temperature STM/AFM. The variety of modes in which the device was successfully operated in exemplifies the wide range of possible use-cases, and shows that the haptic SPM controller is an effective way to feel, simulate, and interact with nano-scale features.

Such a device could be especially useful for educational and accessibility purposes. Tactile feedback can help develop more intuition about the operational principles of SPM technology than sight-based methods, due to the analogous nature of operation and the near-instantaneous feedback experienced by the user. Scanning probe microscopy is essential for the study of nano-scale environments, and further refinement of haptic SPM controllers will only serve to make interacting with such instruments more ergonomic and more accessible to the layperson.

## REFERENCES

- <sup>1</sup>T. B. Sheridan, *Telerobotics, automation, and human supervisory control* (MIT press, 1992).
- <sup>2</sup>Y. Hatamura and H. Morishita, in *IEEE Proceedings on Micro Electro Mechanical Systems, An Investigation of Micro Structures, Sensors, Actuators, Machines and Robots*. (IEEE, 1990) pp. 203–208.
- <sup>3</sup>R. Hollis, S. Salcudean, and D. Abraham, in *IEEE Proceedings on Micro Electro Mechanical Systems, An Investigation of Micro Structures, Sensors, Actuators, Machines and Robots*. (1990) pp. 115–119.
- <sup>4</sup>R. Taylor, J. Chen, S. Okimoto, N. Llopis-Artime, V. Chi, F. Brooks, M. Falvo, S. Paulson, P. Thiansathaporn, D. Glick, S. Washburn, and R. Superfine, in *Proceedings. Visualization '97 (Cat. No. 97CB36155)* (1997) pp. 467–470.
- <sup>5</sup>M. Falvo, G. Clary, A. Helser, S. Paulson, R. Taylor, V. Chi, F. Brooks, S. Washburn, and R. Superfine, *Microscopy and Microanalysis* **4**, 504–512 (1998).
- <sup>6</sup>M. Sitti and H. Hashimoto, in *Proceedings. 1998 IEEE/RSJ International Conference on Intelligent Robots and Systems. Innovations in Theory, Practice and Applications (Cat. No. 98CH36190)*, Vol. 3 (IEEE, 1998) pp. 1739–1746.
- <sup>7</sup>M. Guthold, M. Falvo, W. Matthews, S. Paulson, J. Mullin, S. Lord, D. Erie, S. Washburn, R. Superfine, F. Brooks, and R. Taylor, *Journal of molecular graphics & modelling* **17**, 187–197 (1999).
- <sup>8</sup>M. Reiner, *Interactive Learning Environments* **7**, 31 (1999), <https://doi.org/10.1076/ilee.7.1.31.3598>.
- <sup>9</sup>M. Guthold, M. Falvo, W. Matthews, S. Paulson, S. Washburn, D. Erie, R. Superfine, F. Brooks, and R. Taylor, *IEEE/ASME Transactions on Mechatronics* **5**, 189 (2000).
- <sup>10</sup>F. J. Rubio-Sierra, R. W. Stark, S. Thalhammer, and W. M. Heckl, *Applied Physics A* **76**, 903 (2003).
- <sup>11</sup>M. Sitti and H. Hashimoto, *IEEE/ASME transactions on mechatronics* **8**, 287 (2003).
- <sup>12</sup>M. Jobin, R. Foschia, S. Grange, C. Baur, G. Gremaud, K. Lee, L. Forró, and A. Kulik, *Review of Scientific Instruments* **76**, 053701 (2005), <https://doi.org/10.1063/1.1891346>.
- <sup>13</sup>Y.-A. Lim, C. G. Lee, J.-P. Kim, and J. Ryu, in *2009 IEEE International Symposium on Industrial Electronics* (IEEE, 2009) pp. 983–988.
- <sup>14</sup>H. Xie, D. S. Haliyo, and S. Régnier, *Nanotechnology* **20**, 215301 (2009).
- <sup>15</sup>J. Hou, L. Liu, Z. Wang, Z. Wang, N. Xi, Y. Wang, C. Wu, Z. Dong, and S. Yuan, *IEEE Transactions on Automation Science and Engineering* **10**, 285 (2013).
- <sup>16</sup>A. Schmid, R. Yechangunja, S. Thalhammer, and M. A. Srinivasan, in *2012 IEEE Haptics Symposium (HAPTICS)* (2012) pp. 517–522.
- <sup>17</sup>F. Marchi, S. Marlière, D. Urma, J.-L. Florens, J. Chevalier, C. Cadoz, and A. Luciani, in *mICTE2005* (2005) pp. 510–515.
- <sup>18</sup>B. Tse, W. Harwin, A. Barrow, B. F. A. Quinn, M. J. Cox, et al., in *Haptics: Generating and Perceiving Tangible Sensations: International Conference, Eurohaptics 2010, Amsterdam, July 8–10, 2010. Proceedings* (Springer Berlin Heidelberg, 2010) pp. 101–108.
- <sup>19</sup>A. Bolopion, G. Millet, C. Pacoret, and S. Régnier, *Reviews of Human Factors and Ergonomics* **9**, 57 (2013), <https://doi.org/10.1177/1557234X13503293>.
- <sup>20</sup>G. Millet, A. Lécuyer, J.-M. Burkhardt, S. Haliyo, and S. Régnier, *International journal of human-computer studies* **71**, 608 (2013).
- <sup>21</sup>C. Pacoret, R. Bowman, G. Gibson, S. Haliyo, D. Carberry, A. Bergander, S. Régnier, and M. Padgett, *Optics express* **17**, 10259 (2009).
- <sup>22</sup>C. Pacoret, A. Bergander, and S. Régnier, in *International Conference on Human Haptic Sensing and Touch Enabled Computer Applications* (Springer, 2010) pp. 333–338.
- <sup>23</sup>C. Pacoret and S. Régnier, *Review of Scientific Instruments* **84**, 081301 (2013).
- <sup>24</sup>L. M. A. Perdigão and A. Saywell, *Review of Scientific Instruments* **82**, 073704 (2011), <https://doi.org/10.1063/1.3600572>.
- <sup>25</sup>M. F. Green, T. Esat, C. Wagner, P. Leinen, A. Grötsch, F. S. Tautz, and R. Temirov, *Beilstein journal of nanotechnology* **5**, 1926 (2014).
- <sup>26</sup>P. Leinen, M. F. Green, T. Esat, C. Wagner, F. S. Tautz, and R. Temirov, *JoVE (Journal of Visualized Experiments)*, e54506 (2016).
- <sup>27</sup>W. Vogl, B. K.-L. Ma, and M. Sitti, *IEEE transactions on nanotechnology* **5**, 397 (2006).
- <sup>28</sup>W.-H. Soe, C. Manzano, A. De Sarkar, N. Chandrasekhar, and C. Joachim, *Physical review letters* **102**, 176102 (2009).
- <sup>29</sup>J. Repp, G. Meyer, S. M. Stojković, A. Gourdon, and C. Joachim, *Physical Review Letters* **94**, 026803 (2005).
- <sup>30</sup>J. Itatani, J. Levesque, D. Zeidler, H. Niikura, H. Pépin, J.-C. Kieffer, P. B. Corkum, and D. M. Villeneuve, *Nature* **432**, 867 (2004).
- <sup>31</sup>X. Lu, M. Grobis, K. Khoo, S. G. Louie, and M. Crommie, *Physical Review Letters* **90**, 096802 (2003).
- <sup>32</sup>L. Gross, F. Mohn, N. Moll, P. Liljeroth, and G. Meyer, *Science* **325**, 1110 (2009).
- <sup>33</sup>L. A. Jones and H. Z. Tan, *IEEE transactions on haptics* **6**, 268 (2012).
- <sup>34</sup>L. Bartels, G. Meyer, and K.-H. Rieder, *Applied Physics Letters* **71**, 213 (1997).
- <sup>35</sup>W. P. Davey, *Physical Review* **25**, 753 (1925).